Interfacial water dielectric-permittivity-profile measurements using atomic force microscopy

O. Teschke,[1,*] G. Ceotto,[2] and E. F. de Souza[3]
[1]*Nano-Structures Laboratory, IFGW/UNICAMP, 13081-970, Campinas, São Paulo, Brazil*
[2]*Departamento de Física, Universidade Federal de Viçosa, 36571-000, Viçosa, MG, Brazil*
[3]*Instituto de Ciências Biológicas e Química, Pontifícia Universidade Católica de Campinas, 13020-904, Campinas, São Paulo, Brazil*
(Received 19 January 2001; published 27 June 2001)

The arrangement of water molecules at charged aqueous interfaces is an important question in biology, electrochemistry, and geochemistry. Theoretical studies suggest that the molecules become arranged in several layers adjacent to a solid interface. Using atomic force microscopy we have measured the water dielectric-permittivity profile perpendicular to mica surfaces. The measured variable permittivity profile starting at $\epsilon \approx 4$ at the interface and increasing to $\epsilon = 80$ about 10 nm from the surface suggests a reorientation of water molecule dipoles in the presence of the mica interfacial charge.

DOI: 10.1103/PhysRevE.64.011605 PACS number(s): 68.08.−p, 68.37.Ef, 77.22.Ch, 77.55.+f

I. INTRODUCTION

The nanometer-scale structure of liquid films is a fundamental subject of materials and biological sciences that has until now eluded direct study because of the lack of suitable microscopy techniques with the required level of resolution. The interfacial structure of thin films of water is an important and largely unsolved problem in physics, chemistry, and biology. Water films alter the adhesion and lubricating properties of surfaces and the reactivity of solids with ambient gas molecules. The contact angle of water is used as a measure of the chemical activity of the surface. In biological processes, water films are critical for ion transport. Several studies have recently been devoted to the layering and orientation of water molecules on surfaces [1–4].

Over recent decades a great deal of insight into interfacial water molecules has been gained from theoretical studies especially those with numerical simulations [5]. Experimental research on the topic, however, has been limited. Measurements of forces between two surfaces immersed in aqueous solution, but separated at molecular distances, seem to indicate that water molecules at the surfaces have both translational and orientational order [6]. Nuclear magnetic resonance studies also show some evidence that water molecules at surfaces behave differently from in the bulk [7]. Optical second harmonic generation and sum-frequency generation have recently been proved to be adequate tools for investigation of liquid interfaces [8–10]. They show that water molecules near a charged surface are strongly oriented [9].

Although modern scanning probe microscopes, like the scanning tunneling microscope and the atomic force microscope (AFM), have atomic-scale resolution, they cannot be easily used to study interfacial layers on surfaces. If the probe tip comes into contact with the surface, strong capillarity forces will cause the liquid to wet the tip and will strongly perturb the liquid. To avoid the bulging of the liquid surface that leads to wetting and capillary interaction, the tip must be kept at least several tens of angstroms from the imaging surface. Recently Hu *et al.* [11] have been able to image structures formed by the bilayer or monolayer deposition of water on mica surfaces. Because polarizability is a material property, when layers of one material are imaged on a substrate of a different material, the apparent height or image contrast is modified by the electric permittivity of the material being imaged. For molecularly thin layers, the ratio between real and apparent heights can differ by a factor of order 10 [11].

In this paper, we present our work on the dielectric-permittivity profile of interfacial water, obtained by AFM microscopy, at mica-water interfaces. The profile is measured using the force acting on an uncharged tip when immersed in the mica-water double layer. The force acting on the tip is modeled by the gradient of the electrostatic energy variation involved in the immersion of the tip with dielectric permittivity ϵ_{tip} in the double-layer region with ϵ_{DL}. Both the long-range component ($\sim$ Debye length) and the force acting at a few angstroms from the interface are fitted to the measured experimental curves.

Previous studies of interfacial water molecular distribution

Water molecules are ordered by the surface according to two principles: first they effectively compensate for the local dipolar charge distribution of the surface molecules, and secondly they reorient themselves due to the geometric constraints of the surface [12]. Owing to the diminished possibilities for making favorable hydrogen bonds, the water molecules closest to the surface orient themselves in such a way as to optimize their interwater hydrogen bonds. What is then the water structuring effect in the vicinity of a charged surface? Water molecules reorient themselves in such a way that not only is the local electrostatic field being compensated for, but in addition the interwater hydrogen bonds are optimized, resulting in a region with a more aligned molecular distribution than in the bulk and consequently a layer with a lower dielectric permittivity than in the bulk.

The orientational polarization of water was originally identified as the ''order'' parameter in the Landau-type expansion of the Gibbs energy density in the early model of Marcelja and Radic [13]. Although this phenomenological approach is definitely an oversimplification, the orientational

*Electronic address: oteschke@ifi.unicamp.br

polarization remains the most direct way to characterize the order. Etzler [14] has proposed a statistical thermodynamic model for interfacial water. The model discusses the structure of water in terms of both a bond percolation model for bulk water (as proposed by Stanley and Teixeira [15]) and a single-particle enthalpy distribution calculated earlier by Stey [16]. Two recent models, one by Cevc [17] and the other by Lipowsky and Grotehans [18], incorporate both solvent and surface properties. Both models treat the interface as an interphase, i.e., in three dimensions. The Cevc model assumes that the ordering of water is directly related to the electrostatic interactions in the interface.

It is obvious then that the interfacial water polarization distribution in the immediate surrounding of a solid surface is different from that in bulk water. The big questions are how different is it and how far from the surface do these differences persist? The existence of long-range repulsions between surfaces in water due to structural ordering of water molecules has long been recognized; although there has been much disagreement over the years on whether the effective range of this modified structure is small (a few angstroms) or large (a few thousand angstroms) [19]. Palmer *et al.* [20] found that the dielectric permittivity of water separated by thin mica plates decreased with the thickness of the film from more than 20 for films about 5 μm in thickness to less than 10 for films about 2 μm in thickness. Metzik *et al.* [21] measured very low ϵ values for water films between mica sheets, for example, $\epsilon=4.5$ at $H=70$ nm. Bockris and Reddy [22] and Kaatze [23] suggest that for a fully oriented primary water layer the dielectric permittivity is about 4 as compared to a bulk value of ~ 80. Thicknesses of layers of bonded water in which molecules are suitably oriented, according to Derjaguin [24] and Churaev *et al.* [25], can correspond to 100 nm.

In the past, experiments were performed in order to measure the interfacial water index of refraction at optical frequencies. Recently this experiment was repeated by Kékicheff and Spalla [26] and the value measured at the interface was exactly equal to the bulk value. This result is expected when interfacial water is probed by electromagnetic radiation at a wavelength corresponding to the visible region and it is explained as follows. For nonpolar dielectric substances the lowest frequency ν_0 at which appreciable absorption occurs is usually in the visible or in the ultraviolet region. Thus for $\nu<\nu_0$ the dielectric permittivity ϵ should be equal to the static dielectric permittivity and should satisfy the Maxwell relation $\epsilon=n^2$. However, polar substances display optical as well as infrared polarization. Water consisting of dipolar molecules in addition also shows polarization due to dipolar orientation. The calculation of the water dielectric permittivity uses Kirkwood's formula,

$$\epsilon-n^2=\frac{\epsilon}{2\epsilon+n^2}\frac{N_0\mu\mu^*}{\epsilon_0 k_{\mathrm{B}}T},$$

where $\mu\mu^*=g\mu^2$, and g is the Kirkwood orientation correlation factor. Since the water refractive index $n^2\ll\epsilon$, then

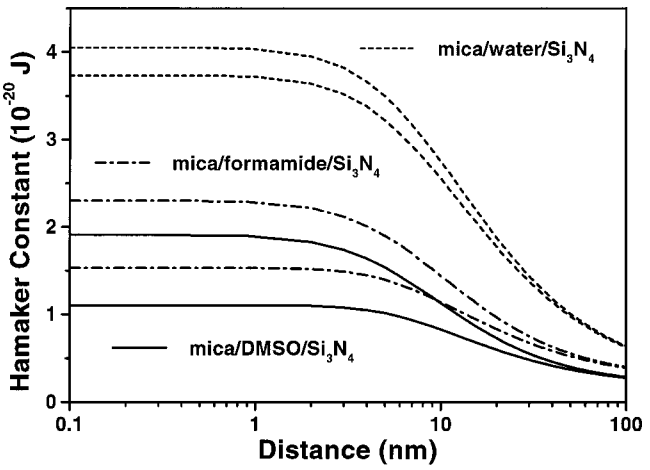

FIG. 1. Calculated Hamaker constants as a function of the distance to the surface for mica solution and Si_3N_4 tip. Configuration: water (dashed line), formamide (dashed-dotted line), and DMSO (full line).

$$\epsilon\approx\frac{7(n^2+2)^2 g_w\mu^2 N_0}{54\,\epsilon_0\,k_B T}=78.4$$

when $g_w=2.82$, $\mu=6.18\times10^{-30}$ C m is the dipole moment, $N_0=(N_A\rho/M)=3.35\times10^{28}$ m^{-3} ($N_A=6.02\times10^{23}$ mol^{-1} is the Avogadro number, $\rho=1$ g/ml is the density, $M=18$ g/mol is the molecular weight), the Boltzmann constant $k_B=1.38\times10^{-23}$ J/K, and $T=298$ K. The result compares favorably with the experimental value 78.5.

In order to measure the possible contribution of the water polarization effect at the interface, an attraction that exceeds the van der Waals (vdW) attraction has to be present. The vdW attraction contribution will be discussed in the next paragraphs.

The Hamaker constant was determined as follows. The calculations are based on the procedure outlined in Ref. [27]. We used a generalization of Hamaker's approach where the Hamaker constant is redefined according to $A(H,T)=A_{\nu=0}(T)+A(H)$, and $A(H)$ takes into account dispersion interactions. It is calculated by means of the microscopic approach and includes the correction for retardation effects in vacuum. This correction depends on the shape of the interacting bodies. Vassilieff and Ivanov (cited in Ref. [27]) reduced the results from the macroscopic theory to an effective interaction between two bodies denoted by 1 and 2, immersed in a third dielectric medium 3. The calculated Hamaker constant dependence on distance for water, dimethylsulfoxide (DMSO), and formamide, is shown in Fig. 1.

The interaction energy associated with the vdW attraction of a conical tip with a spherical end and a flat surface is calculated by the expression below [28]:

$$W(H,T)=-\frac{2A(H,T)}{(n-2)(n-3)}(W_{\mathrm{SS}}+W_{\mathrm{TC}}), \qquad (1a)$$

where

$$W_{SS}=\int_0^R \frac{(2R-z)z}{(H+z)^{n-3}}\,dz,$$

and

$$W_{TC}=\int_0^{(3\kappa^{-1}-R-H)} \frac{[R+(\tan\alpha)z]^2}{(H+z)^{n-3}}\,dz$$

are the semispherical end and truncated-conical tip contributions, respectively; and where z is the integration variable of the trapezoidal volume, H is the distance between the surface and the end of the tip, and α is the cone-shaped tip vertex angle. The value of $F_{vdW}(H,T)$ (for van der Waals force $\Rightarrow n=6$) is

$$F_{vdW}(H,T)=-\frac{\partial W(H,T)}{\partial H}. \tag{1b}$$

For the repulsive term we used the same simple analytical expression for electrostatic force derived by Butt [29] for a sharp conical tip with a spherical end, which, for $\sigma_{tip} \ll \sigma_{mica}$, is

$$F_e=\frac{\pi\sigma_{mica}^2}{\epsilon_0\epsilon\kappa^2}\exp(-2\kappa H)G, \tag{2}$$

where the geometric factor G is

$$G=2\kappa R-1+e^{-2\kappa R}e^{2\kappa R\sin\alpha}(1+\tan^2\alpha).$$

The fitting of the above expression to the experimental points is adjusted by varying the parameter κ and σ_{mica}.

The combination of Eqs. (1b) and (2) is the essence of the DLVO theory, where $F=F_{vdW}+F_e$. Both the vdW force and the electrostatic force were calculated using the MATHEMATICA 4 program for water, DMSO, and formamide and fitted to the experimental points.

II. EXPERIMENT

The atomic force microscope is the most adequate equipment available for measuring interfacial force with a spatial resolution of a few angstroms in the scanned plane and 0.1 Å in the normal direction to the scanned plane. If we use soft cantilevers with a spring constant of 0.03 N/m the force resolution in the normal direction to the scanned plane is $(0.03N\,m^{-1})\times 0.1\times 10^{-10}$ m$=0.3$ pN. Various options of tips and substrates are possible. In this work we used neutral tips ($Si_3N_4\Rightarrow\epsilon=7.4$) and charged surfaces (mica) as well as metallic-coated tips ($\epsilon\approx\infty$) and mica surfaces.

In our experiments a commercial AFM instrument, Topometrix TMX2000, was used where the movement of the cantilever was detected by the conventional deflection sensor using a four-quadrant detector enabling vertical as well as lateral force measurements. A special cell was built in order to perform observations in liquid media [30]. The cell was made of Teflon™ and the sample is fixed at its bottom. It is moved in the x, y, and z directions with respect to a stationary tip. The laser beam enters and leaves the cell through a glass plate and thus does not cross the air-liquid interface, which is usually curved. The top-confining surface of the solution in the cell is far removed from the cantilever beam. In this geometry the displaced liquid follows a path that is perpendicular to the cantilever beam. Water (Milli-Q Plus quality, resistivity ~ 15 MΩ/cm), dimethylsulfoxide, formamide, NaCl, and KCl solutions were introduced into the cell after freshly cleaved mica was mounted on the xyz translator of the AFM. The experiments were performed at a temperature of 20 °C. Each curve presented was registered using at least five different mica substrates and three different tips with various approach velocities averaged using measurements at different points of the sample. Airborne contamination is minimized by preparing samples in a compact laminar flow cabinet and scanning samples in a clean air hood. Forces between commercial silicon nitride ($\epsilon_{tip}=7.4$) tips and flat mica surfaces ($\epsilon_{mica}=5.4$) [31] were measured after 1, 24, and 36 h of immersion in water. Identical force vs distance curves was registered, showing no evidence of tip aging.

A. Mica surface

Mica is always negatively charged in water. When the mica basal plane is placed in water, the mechanism for the formation of the double layer is assumed to be the dissolution of K^+ ions as well as ion exchange of K^+ by H^+ or H_3O^+ ions. It should be noted that the K^+ ions initially held on the mica surface in the high resistivity water (18 MΩ/cm, $\sim 5\times 10^{-6}M$ 1:1 electrolyte at pH~ 6) should be at least partially H_3O^+ ion exchanged. Considering that the solvent volume of the cell was 300 μl and the mica exposed area was 1.13 cm^2, if all K^+ ions on the mica surface were exchanged into solution, the K^+ concentration would be about $8.3\times 10^{-8}M$, almost two orders of magnitude smaller than the calculated concentration of the H_3O^+ present in the solution. The charge residing within the double layer has the same net magnitude as but opposite sign to the charge present at the mica surface. The ζ potential at the macroscopic mica-surface–water interface was measured using the plane-interface technique in the presence of $10^{-3}M$ KCl, and was found to be ~ 125 mV within the pH range from 5 to 6 [32].

B. Tips

We have obtained best results in measurements with very soft cantilevers with silicon nitride tips, typically ~ 0.03 N/m (Microlever™, type B, ThermoMicroscopes). Verifications of the spring constants of the cantilever by the method of Sader *et al.* [33] gave values not statistically different from the manufacturer's values.

The commercial silicon nitride tip surface has been found to be close to electrically neutral over a wide pH range (from at least pH 6 to 8.5), thus indicating equal densities of silanol and silylamine surface groups [31]. The surface of a silicon nitride tip in aqueous solution is composed of amphoteric silanol and basic silylamine [secondary (silazane, $—Si_2NH_2$) and possibly primary (silylamine, $—SiNH_3$) amines although the latter is rapidly hydrolyzed] surface

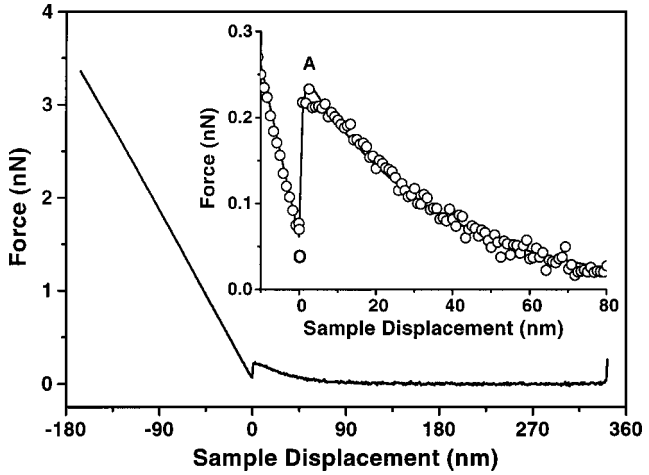

FIG. 2. Force vs sample displacement curve for a Si_3N_4 tip and a mica sample immersed in water. Inset: Extended scale showing the region close to the interface. Experimental points shown by (○). Full line to guide eye.

groups [34] at pH$\sim$6; with no added electrolyte the silicon nitride surface is either zwitterionic (zero net charge) or slightly negatively charged [35]; consequently, we assumed that the surface charge density in the tip $\sigma_{\mathrm{tip}} \ll \sigma_{\mathrm{mica}}$ in water (pH$\sim$6.3). To verify the surface charging behavior of the tips, force vs separation curves in solutions with pH between $\sim$5.2 and 6.8 were measured, and the isocharging point (ICP) for silicon nitride was determined to be $p\mathrm{H}_{\mathrm{ICP}} \approx 6.3$.

Silicon and metal (platinum iridium and cobalt) coated tips were also used. These conical tips (Ultralevers, ThermoMicroscopes) are mounted in hard cantilevers with nominal spring constants of 0.26 and 3.3 N/m, respectively.

C. Tip radius of curvature estimate

The radius of the tip was characterized by the observation of porous silicon structures and by comparing the size of the measured silicon particles by transmission electron microscopy (TEM) and AFM [36]. This comparison allows us to estimate the distortion of the AFM images due to the finite size of the tip radius. The estimate of the radius is obtained by deconvolution of the measured profile curve and comparison with the particle diameter measured by TEM. The determined values are in agreement with the value given by ThermoMicroscopes technical information sheets. The selected Si_3N_4 supertips have an $\sim$5 nm tip radius of curvature while Si tips have a 10 nm and Co- and Pt-coated tips have an $\sim$25 nm tip radius of curvature.

III. RESULTS AND DISCUSSION

For a neutral Si_3N_4 tip and charged mica surface in water a typical force vs sample displacement curve is shown in Fig. 2. The vertical axis represents the force acting between tip and sample surface. It is obtained by multiplying the deflection of the cantilever by its spring constant. The horizontal axis represents the distance the sample is moved up and down by the xyz translator. In this curve repulsive and attractive forces act between tip and sample before contact. Hence, when the sample approaches the tip, the cantilever bends upward. At a certain point A the tip is attracted to the surface. Finally, moving the sample still further causes a deflection of the cantilever by the same amount the sample is moved. The dashed line starting at point O where the tip is in contact with the sample represents this. The approaching force curve (Fig. 2) collected on a mica surface in water is a plot of the change in cantilever deflection (ΔY) vs sample displacement (ΔX). On a hard nondeformable surface, ΔY is proportional to ΔX while the tip and the sample are in contact. Rather than using sample position (X), it is more useful to use an absolute distance (H) that is relative to the separation between the tip and the sample surface. The correction to produce a force-distance curve uses the relationship $H = \Delta X + \Delta Y$ [37]. The following force curves show the force vs absolute distance plots.

Figure 3(a) shows the force vs distance curve measured with a silicon nitride tip on mica obtained at a $10^{-3}M$ NaCl concentration, Fig. 3(b) that at a $10^{-3}M$ KCl concentration, and Fig. 3(c) that at a $10^{-3}M$ LiCl concentration. The force vs distance curves were also measured for various salt concentrations. For $0.1M$ NaCl solution forces act on the tip at smaller distances away from the mica surface than for $10^{-3}M$ NaCl, but larger than for $1.0M$ solutions. These observations indicate that these forces are the result of the presence of a double layer. For $1.0M$ NaCl solution, where the expected double-layer thickness is <5 nm, the repulsive force described above when the tip was approaching the surface was not detected, indicating that this force is not derived from thin film viscosity or compression effects. Figures 4(a) and 4(b) show the tip approach for DMSO and formamide, respectively. Observe that there is no jump onto the surface as is present in the water-measured curve (point A in Fig. 2).

Force vs separation curves were then measured for tips with different dielectric constants. Figure 5(a) shows the force vs sample position curves for silicon tips ($\epsilon = 11.6$) and for silicon nitride tips ($\epsilon = 7.4$) immersed in the mica double layer. Platinum- and cobalt-coated tips ($\epsilon \approx \infty$) were then used and the force vs separation curves are shown in Fig. 5(b). Different force curves were measured when compared to the ones measured for silicon and silicon nitride tips. The difference observed is an attraction of the tip at distances far away from the interface when compared to the repulsion observed for silicon and silicon nitride tips. In the next section we are going to model the force acting on the tip and call it the dielectric exchange force.

A. Dielectric exchange force

The analysis of the force acting on the cantilever is as follows. One side of the cantilever is gold covered; therefore there is a charge difference between the cantilever surfaces, which may cause cantilever deformation or deflection. However, this deflection is present throughout the duration of the approach and adds to the baseline force. The influence of the cantilever charge on the measured force variation during the tip approach to the surface is negligible since the Debye-Hückel length of mica immersed in Milli-Q water is around 100 nm and the tip height is ~ 3 μm. Therefore, only the tip

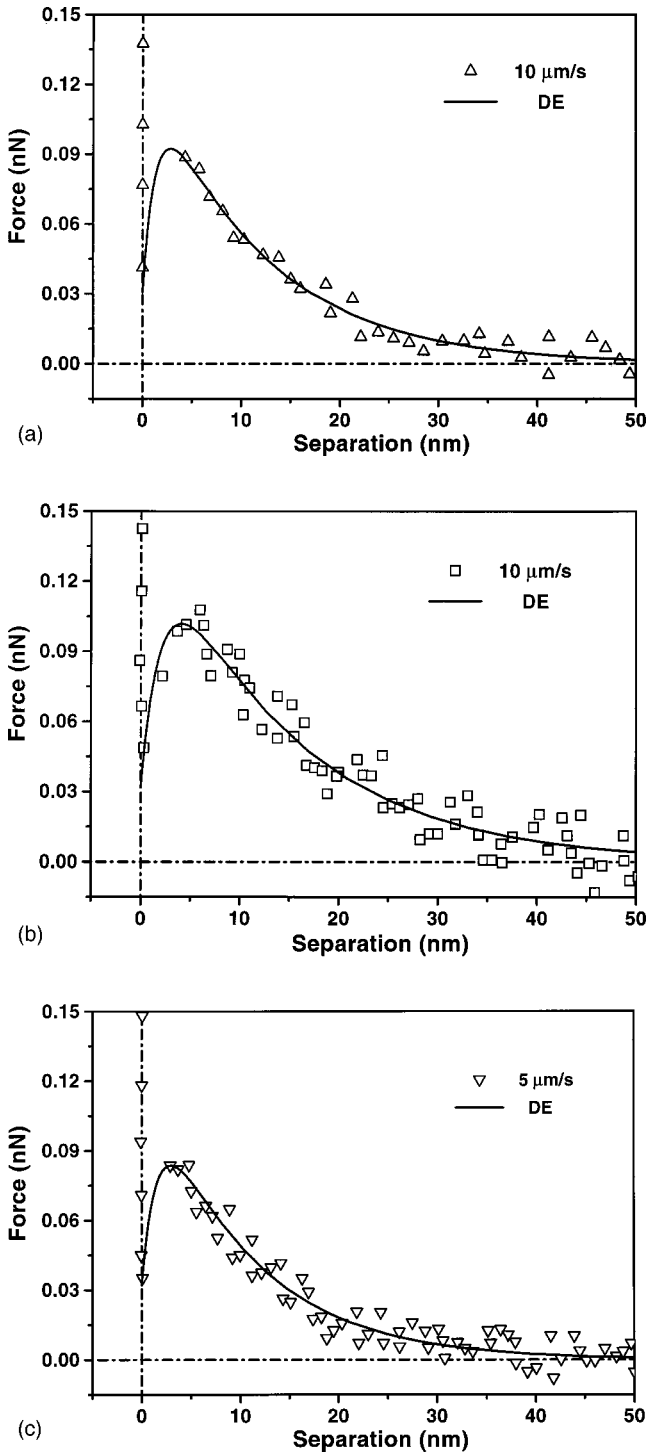

FIG. 3. Force vs separation curve for a Si_3N_4 tip and a mica sample immersed in (a) $10^{-3}M$ NaCl, (b) $10^{-3}M$ KCl, and (c) $10^{-3}M$ LiCl. DE indicates the curve calculated from the dielectric exchange force [Eq. (3) below].

is immersed in the mica double-layer region. Supertips used in these experiments are sharpened conical tips with an α apex angle ($\sim 12°$ for Si, Co, and Pt tips and $\sim 18°$ for Si_3N_4 tips) ~ 100 nm in height etched at the end of ~ 3 μm height tips. Consequently, the main interaction region of the tip/cantilever with the mica double layer is the sharpened

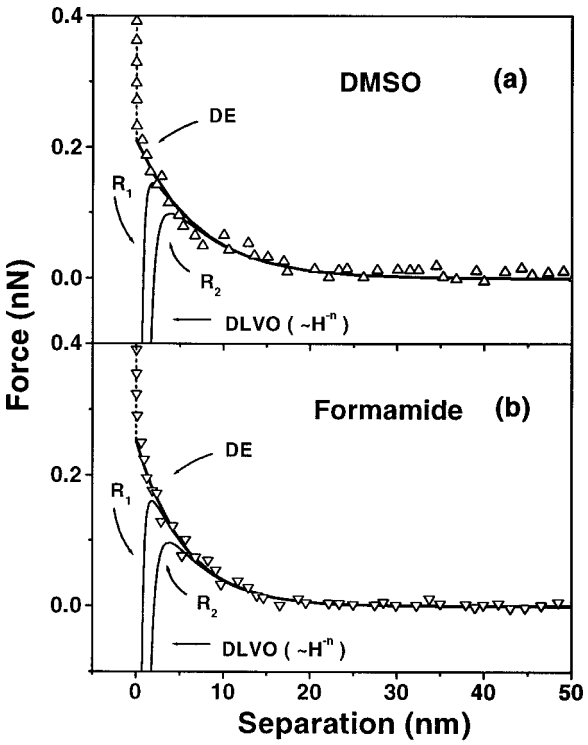

FIG. 4. Force vs absolute tip-substrate distance curve for a Si_3N_4 tip and mica sample immersed in (a) dimethylsulfoxide and (b) formamide. The full line corresponds to the fitting by Eq. (3) using the parameters shown in Table I below. The dashed line indicates the region where tip and substrate are in contact. Also shown are calculated force vs separation curves by Eq. (3) below, indicated by DE (dielectric exchange force), and DLVO theory, indicated by DLVO.

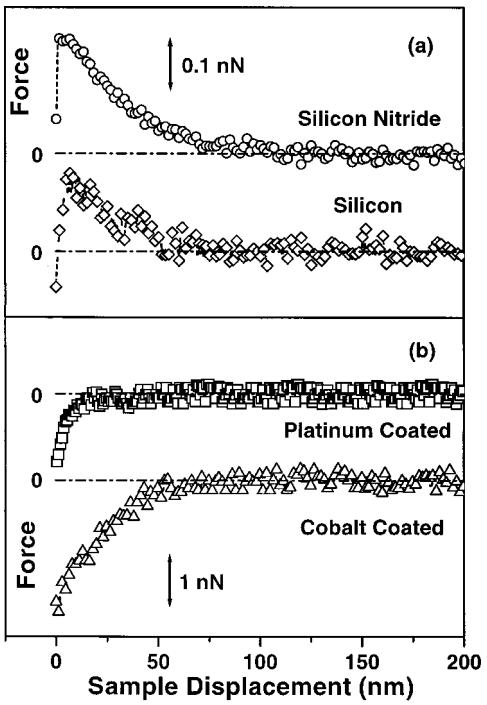

FIG. 5. Force vs. separation curves measurements for tips with various dielectric permittivities: a) silicon, silicon nitride and b) cobalt coated and platinum iridium coated tips.

region of the tip and the force variation measured by the AFM during the tip immersion in the mica surface double layer is the force experienced by the tip.

The electrostatic energy density then is written as a function of the electric displacement vector [38,39]. We also assume that the displacement vector is equal to the field of an infinite plane and that the tip shape does not influence this field. A simple analytical expression for the electrostatic force was derived based on the following principle: it is energetically favorable for a surface charge to be surrounded by a medium with large dielectric permittivity like water. If the tip approaches the double-layer region it replaces the water and since the tip material has a lower dielectric permittivity than water the configuration becomes energetically unfavorable. Consequently, the tip is repelled by the double-layer charge. Based on the previous arguments, conducting tips, which have infinite static permittivity, should be attracted by the charged surface. To estimate the size of this exchange repulsion force we assumed, for a measured double-layer width, that the energy change involved in the immersion of the sharpened conical-shaped tip inside the double layer, is given by the product of the immersed tip volume times the dielectric permittivity variation and times the square of the electric displacement vector. The tip was defined to have a sharpened conical shape with one flat end with an area of πR^2 (see Fig. 6). A schematic diagram of a truncated cone compared to a cone with a spherical tip end is shown in the inset of Fig. 6. Since our model proposes that the force on the tip is associated with the tip immersion in the electric field generated at the mica interface, and the double-layer width is $\sim$100 nm, the effect of a 5 nm radius spherical end tip when compared to a truncated conical tip with a 5 nm flat end radius is negligible. The difference in cross sections is indicated by the dashed area. Numerical calculations support our claims.

The double layer is characterized by the surface ionic charge distribution and the Debye-Hückel length is given by

$$\kappa^{-1}=\sqrt{\frac{\epsilon_0\,\epsilon_{\rm bulk}\,k_{\rm B}T}{e^2\sum\, n_i^{\infty}Z_i^2}},$$

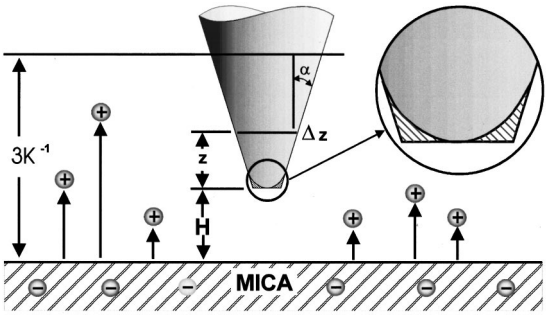

FIG. 6. Conical-shaped tip with a cone angle α and a flat end with an area of πR^2 immersed in the double-layer region z is the integration variable of the elemental volume with width Δz and H is the distance between the surface and the end of the tip. Inset: Schematic diagram of a truncated cone with one flat end compared to a cone with a spherical tip end. The dashed region indicates the difference in cross sections.

where e is the electronic unit charge, n_i^{∞} is the ion density in the bulk solution, and Z_i represents the valency. The sum is over all species of ions present. The *electric displacement vector* $(\vec{D})$ is assumed to have an exponential spatial dependence $D(z)=D_0\exp(-\kappa z/2)$, where the displacement vector amplitude (D_0) is determined by the ionic charge distribution at the mica surface by using Gauss's law. A schematic diagram of the tip immersion in the double-layer region is depicted in Fig. 6, where z is the integration variable of the trapezoidal volume and H is the distance between the surface and the end of the tip. The elemental volume (dv) of the trapezoidal tip immersed in the double-layer region is given by $dv=\pi[R+(\tan\alpha)\,z]^2dz$ and the change in the electric energy involved in the exchange of the dielectric permittivity of the double layer with that of the tip is calculated by integrating the energy expression over the tip immersed volume in the double-layer region. The force is obtained by the gradient of the energy expression, i.e., $F_z=-\,\mathrm{grad}\,\Delta E$, where

$$\Delta E=\frac{1}{2}\int_0^{10\kappa^{-1}-H}\left[\frac{1}{\epsilon_{\rm DL}(z)}-\frac{1}{\epsilon_{\rm tip}}\right]\frac{D^2(z)}{\epsilon_0}\times\pi\,[R+(\tan\alpha)\,z]^2\,dz \tag{3}$$

and the integration upper limit is 10 Debye lengths minus the tip-substrate distance. Several estimates have been given in the literature for the dielectric-permittivity dependence on the distance to the liquid-solid interface in the electric double layer: Gur *et al.* [40] propose the introduction of a variable dielectric permittivity into the Poisson-Boltzmann equation and the explicit expression of the dielectric saturation $\epsilon(E)$ is

$$\epsilon(E)=n^2+(\epsilon_{\rm bulk}-n^2)\,(3/\beta E)\,L(\beta E),$$

where

$$L(\beta E)=\coth(\beta E)-1/(\beta E)$$

is the Langevin function. For water, assuming an optical refractive index $n=1.333$ and a dielectric permittivity in the bulk medium $\epsilon_{\rm bulk}=78.5$ at $T=298$ K, $\beta=5\mu(n^2+2)/2k_BT=1.42\times10^{-8}$ m/V. If we assume an electric field distribution with an exponential decay at the interface $E=E_0\exp(2H/\lambda)$ and using the mica surface charge density $\sigma_{\rm mica}=(1.6\times10^{-19}\ \mathrm{C})/(4.8\times10^{-19}\ \mathrm{m}^2)=0.333\ \mathrm{C\,m^{-2}}$, with the vacuum permittivity $\epsilon_0=8.854\times10^{-12}\ \mathrm{F\,m^{-1}}$, then $E_0=\sigma/2\epsilon_0=1.882\times10^{10}\ \mathrm{N\,C^{-1}}$. Thus the dielectric spatial variation at the interface shows a sigmoidal shape starting at $\epsilon(0)=2.63(>n^2=1.78)$ and increasing to $\epsilon_{\rm bulk}=78.5$ for points far away from the interface.

Podgornik *et al.* [41] propose the following expression for the dielectric permittivity:

$$\epsilon_{\rm DL}(H)=\epsilon_{\rm max}[1+(\epsilon_{\rm max}/\epsilon_{\rm min}-1)\exp(-2H/\lambda)]^{-1}.$$

This expression was used in our work to represent the shape of the dielectric permittivity.

To quantify the characteristic range of the repulsive and attractive forces and to compare the experiments with calcu-

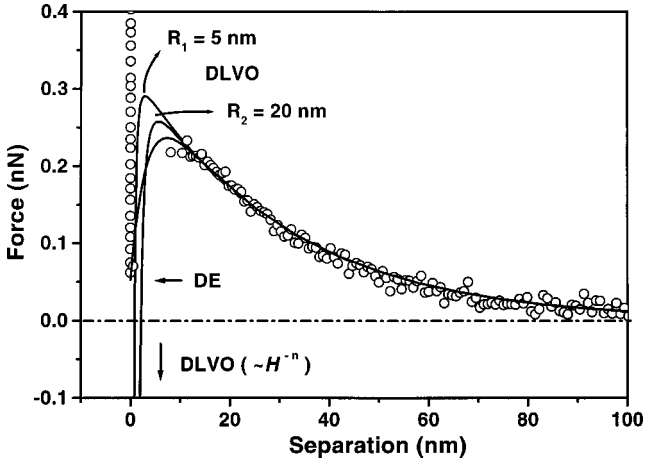

FIG. 7. Force vs absolute tip-substrate distance curve for a Si_3N_4 tip and a mica sample immersed in water. The full line indicated by DE (dielectric exchange force) corresponds to the fitting by Eq. (3), and the full line indicated by DLVO corresponds to fitting by the DLVO theory. Observe that DLVO theory fits the experimental points well only for distances from the interface >10 nm.

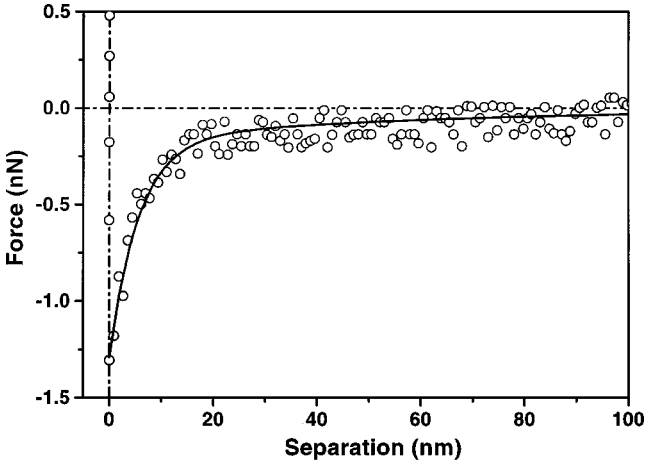

FIG. 8. Force vs absolute separation measurements for a hard cantilever with a platinum-coated tip using the same parameters to fit the experimental data as the ones used for the silicon nitride tips. The full line corresponds to the fitting by Eq. (3).

lations, we tried to fit the repulsive part of the force vs distance curves with the gradient of Eq. (3). Initially, by substituting ϵ_{DL} for ϵ_{bulk}, we fitted the repulsive part of the curve where the adjustment parameters κ^{-1} and D_0 are determined. Then, by adjusting the parameters in the ϵ_{DL} expression it is possible to fit the attractive part of the curve. The best results of the fitting for pure water are shown in Fig. 7 by the full line indicated by DE and the corresponding values are plotted in Table I. Full lines shown in Figs. 3(a), 3(b), and 3(c) for aqueous solutions and in Fig. 4 for DMSO solutions and formamide correspond to the fitting of Eq. (3) to the experimental points. The measured thickness of the diffuse double layer (κ^{-1}) for aqueous solution ($\sim 10^{-6}M$ ion concentration) is ~ 60 nm, in agreement with the value (56 nm) measured by Kékicheff *et al.* [42]. For $10^{-3}M$ NaCl and KCl solutions the calculated values are identical and equal to ~ 10 nm and the measured values are ~ 11 nm [43] and ~ 13 nm, respectively. The values for LiCl, $MgCl_2$, and other solvents are shown in Table I.

B. Dielectric exchange force associated with metal-coated tips

In order to test our hypothesis that the repulsive force acting on the tip at distances $\gtrsim 10$ nm from the interface is associated with the difference of the dielectric permittivity between the solution and the tips we used platinum-coated tips. The measured force vs separation curves for metal-coated tips [Fig. 5(b)] show a different behavior when compared with those observed for silicon nitride tips [Fig. 5(a)]. This is the result of the fact that conductors have an infinite static permittivity, which corresponds to a null electric field inside the tip and, consequently, zero electric energy stored inside the tip volume. The corresponding force on the tip is attractive since the immersion of the tip in the double-layer electric field decreases the total energy of the configuration. The energy variation obtained by the immersion of a metal-coated tip is given by Eq. (3) for $1/\epsilon_{tip} \approx 0$. The fitting of the experimental points to Eq. (3), shown in Fig. 8, was obtained using the same ϵ_{DL} and κ^{-1} values listed in Table I.

TABLE I. Measured parameters of the double layer (for silicon nitride tips).

Solvent	ϵ_{bulk}	κ^{-1} (nm)	ϵ_{DL} (surface)
H_2O	79	60	3.8
$MgCl_2$ $(10^{-3}M)$	79	15	2.5
KCl $(10^{-3}M)$	79	13	7.1
NaCl $(10^{-3}M)$	79	11	3.7
LiCl $(10^{-3}M)$	79	10	8.7
DMSO	46	14	-
Formamide	109	11	-

C. Dielectric exchange force associated with the interfacial water dielectric-permittivity variation

The dielectric exchange force component is also present when the tip is immersed in the water layer close to the mica-solution interface as discussed next. The pure water inner layer dielectric-permittivity value that results in the best fitting of the experimental curve (○) in Fig. 7 is ~ 4, in agreement with the value of 4.2 given in Refs. [23,24]. This decrease of the double-layer dielectric permittivity from its bulk value is associated with the tip attraction near the surface. The attribution of this short-range force in water to surface charge induced change in the water dielectric permittivity accounts for the experimental results shown in this work. The model formulated here, in terms of a reoriented layer of water, predicts an attractive force (or less repulsive force when compared to the double-layer repulsion) that is determined by the degree of polarization of the layer of water molecules at the solid-liquid interface, which decreases the water dielectric permittivity from a value ~ 80 to ~ 4. The experimental points are shown in Fig. 9.

Observe that our model presents good fits of the data at separation distances shorter than 10 nm. The attractive be-

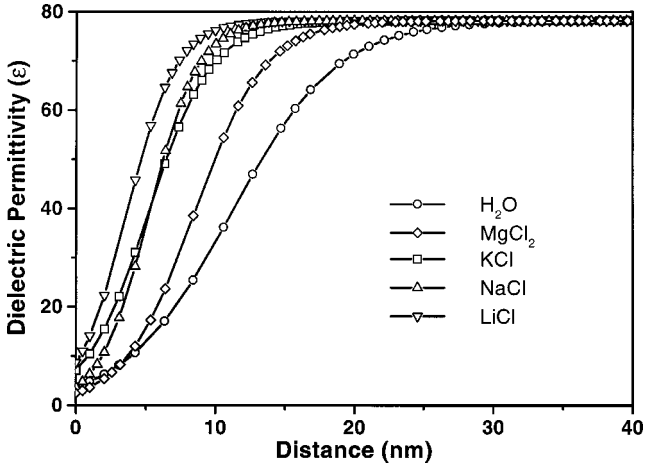

FIG. 9. The full lines correspond to the dielectric-permittivity spatial variation that results in the best fitting to the experimental points.

havior of the tip when immersed in the inner layer is associated with the water dipole partial reorientation at the interface and not the vdW attraction, which has much too short a range (~ 1 nm) [36]. A possible influence of the vdW attractive force on the shape of the force curve was investigated. The vdW force between a flat plate and a conical tip with a spherical end given by Eqs. (1a) and (1b), where the Hamaker constant for a mica substrate and a silicon nitride tip, is calculated by the expression $A(H,T)=A_0+A_1 \exp(-H/H_1)$, where, for water, $A_0=3.81\times10^{-21}$ J, $A_1=3.44\times10^{-20}$ J, and $H_1=19.95$ nm. The calculated force vs distance curves are shown in Fig. 7 for pure water, Fig. 4(a) for DMSO, and Fig. 4(b) for formamide. The vdW attraction decays, $\propto 1/H^n$, are clearly shown to be inadequate to match the attraction force at close distances (<10 nm) to the interface for pure water, DMSO, and formamide.

One point that deserves attention is the low calculated value of the dielectric permittivity of water close to the surface at over $\lesssim 10$ nm distance. In the literature low values of ϵ are expected at distances on the order of a few (~ 6) molecular diameters close to the surface. A few points have to be considered in order to explain the values measured in this work. The classical description [22] of the water inner double layer is based on inner Helmholtz layer capacitance measurements. The saturation layer (reoriented water molecule layer) is determined using capacitance measurements at interfaces in highly concentrated solutions with small κ^{-1} values. A ~ 10 μF/cm^2 capacitance is associated with a hydrated layer thickness of ~ 1 nm and $\epsilon \approx 6$. In these measurements only the ratio of the dielectric permittivity and the layer width is determined; in our work both the distance of the attraction region corresponding to the layer width and the dielectric permittivity are determined simultaneously. If, arbitrarily, we assume the saturation layer width to be the one corresponding to half the maximum amplitude of the dielectric-permittivity variation in Fig. 9, we obtain for Milli-Q water and for $10^{-3}M$ NaCl solutions ~ 8 nm and 3 nm, respectively, for the water dipole reoriented layer width. For highly concentrated solutions ($\sim 10^{-1}M$), the value determined by capacitance measurements is ~ 1 nm [22].

Another point that has to be considered is that the solvation energy calculated using Born's expression is proportional to $(1/\epsilon_0 - 1/\epsilon_{\text{medium}})$. Thus atoms dissociate or adsorb as ions in solution at a rate that is proportional to the inverse difference in dielectric permittivity. This is the first step in the dynamical process. In the next step, to lower even further the energy of the system, water molecules are oriented by the charge of the solvated ions, forming a solvation shell. A similar process happens at the mica surface.

We measured water dielectric-permittivity variations in very dilute solutions and thus layer widths much larger than the ones in concentrated solutions are expected. Water dipoles may be partially oriented in a region close to the interface estimated as follows. For mica immersed in solutions with low ionic concentrations the electric field orients water molecules up to a distance $H=L$ from the interface, given by the expression $k_BT \approx \vec{\mu}\cdot\vec{E}(L)$, where $k_BT \approx 4.11\times10^{-21}$ J is the energy responsible for the thermalization of the molecular orientation distribution of water molecules. The electric displacement vector (D) generated by the mica for fully dissociated surface charges is $D \approx 0.17$ C/m^2. The water dipoles show an orientational effect generated by mica interfacial charges up to ~ 7 nm away from the interface, which corresponds to $\epsilon(L) \approx 27$, calculated using the expression

$$k_BT \approx \frac{\vec{\mu}\cdot\vec{D}(L)}{\epsilon_0 \epsilon(L)},$$

where L is determined using the dielectric permittivity vs distance curve shown in Fig. 9. The evidence for the suggested water dipole reorientation at the interface is associated with the measured variation of the interfacial dielectric permittivity. The interfacial orientation profile of water molecules will be discussed next. Liquid water has an irregular four-coordinated structure but at any instant a molecule may be united with two or three others while some of the remaining members of the coordinated complex are moving toward it and others are moving away from it [44,45]. The four-coordinated water structure predominates in ice at 0 °C but appreciable amounts of the three- and two-coordinated structures are also present. In liquid water from 25 to 90 °C the water molecules are somewhat more than two coordinated.

The structure and orientation of water molecules at an ordered solid surface depends on the solid surface structure [44,45]. The surface unit cell of the muscovite mica basal plane contains one K^+ ion and two distorted hexagonal rings with different Al and Si content. On this surface the water molecules form a fully connected H bond network with the potassium ions within water cages. The presence of potassium does not interrupt the network because the weak solvation energy of K^+ favors a fully hydrogen bonded network over full K^+ solvation. The arrangement of these molecules is mainly determined by the requirement of saturating hydrogen bonds among them and with the core water molecules. The present concept of liquid water indicates that near the solid surface the number of hydrogen bonds per water molecules is higher than in bulk water.

IV. CONCLUSIONS

In summary, both the repulsive and later attractive components of the force acting on the tip during its approach to the surface when immersed in the water double layer are associated with the exchange of a double-layer region with $\epsilon_{DL}(H)$ by the tip with ϵ_{tip}. The dielectric exchange effect gives a consistent description of the force acting on the tip by assuming a double-layer region with a variable polarization profile as a function of the distance to the surface. A relationship of the measured polarization variation at the interface to the reorientation of the water molecular dipoles in the presence of the mica interfacial charge is suggested. Support for the proposed model (dielectric exchange force) is given by the observation of only an attractive component when metallic-coated tips ($\epsilon \approx \infty$) are immersed in the mica double layer. Support for the model of a variable water dielectric permittivity at the interface is given by measurements of only a repulsive force component when a silicon nitride tip is immersed in solvent where there is no interaction between the mica surface and the solvent and, consequently, no solvent structuring at the interface.

ACKNOWLEDGMENTS

The authors are grateful to J. R. Castro and L. O. Bonugli for technical assistance and acknowledge financial support from CNPq Grant No. 523.268/95-5 and FAPESP Grant No. 98/14769-2.

[1] Q. Du, E. Freysz, and Y. R. Shen, Phys. Rev. Lett. **72**, 238 (1994).
[2] J. D. Porter and A. S. Zinn, J. Phys. Chem. **97**, 1190 (1993).
[3] J. N. Israelachvili, Chem. Scr. **25**, 7 (1985); Acc. Chem. Res. **20**, 415 (1987).
[4] J. Glosli and M. Philpott, in *Proceedings of the Symposium Microscopic Models of Electrolyte Interfaces*, Vol. 5 (Electrochemical Society, Pennington, NJ, 1993), p. 90.
[5] S. L. Carnie and G. M. Torrie, Adv. Chem. Phys. **56**, 141 (1984); K. Raghavan, K. Foster, and M. Berkowitz, Chem. Phys. Lett. **177**, 426 (1991); D.A. Rose and I. Benjamin, J. Chem. Phys. **98**, 2283 (1993), and references therein.
[6] R. M. Pashley and J. N. Israelachvili, J. Colloid Interface Sci. **101**, 511 (1984); S. Marcelja and N. Radic, Chem. Phys. Lett. **42**, 129 (1976).
[7] R. Lenk, M. Bonzon, and H. Greppin, Chem. Phys. Lett. **76**, 175 (1980).
[8] P. Guyot-Sionnest, J. H. Hunt, and Y. R. Shen, Phys. Rev. Lett. **59**, 1597 (1988); R. Superfine, J. H. Huang, and Y. R. Shen, Chem. Phys. Lett. **144**, 1 (1991).
[9] S. Ong, X. Zhao, and K. B. Eisenthal, Chem. Phys. Lett. **191**, 327 (1992).
[10] Q. Du, R. Superfine, E. Freysz, and Y. R. Shen, Phys. Rev. Lett. **70**, 2313 (1993).
[11] J. Hu, X.-D. Xiao, D. F. Ogletree, and M. Salmeron, Science **267**, 268 (1995).
[12] D. P. Tieleman and H. J. C. Berendsen, J. Chem. Phys. **105**, 4871 (1996).
[13] S. Marcelja and N. Radic, Chem. Phys. Lett. **42**, 129 (1976).
[14] F. M. Etzler, J. Colloid Interface Sci. **92**, 43 (1983).
[15] H. E. Stanley and J. Teixeira, J. Chem. Phys. **73**, 3404 (1980).
[16] G. C. Stey, Ph.D. thesis, University of Pittsburgh, Pittsburgh, 1967.
[17] G. Cevc, J. Chem. Soc., Faraday Trans. **87**, 2733 (1991).
[18] R. Lipowsky and S. Grotehans, Europhys. Lett. **23**, 599 (1993).
[19] J. N. Israelachvili and G. E. Adams, J. Chem. Soc., Faraday Trans. 1 **74**, 975 (1978).
[20] L. S. Palmer, A. Cunliffe, and J. M. Hough, Nature (London) **170**, 796 (1952).
[21] M. S. Metzik, V. D. Perevertaev, V. A. Liopo, G. T. Timoshtchenko, and A. B. Kiselev, J. Colloid Interface Sci. **43**, 662 (1973).
[22] J. O'M. Bockris and A. K. N. Reddy, *Modern Electrochemistry* (Plenum Press, New York, 1970).
[23] U. Kaatze, J. Solution Chem. **26**, 1049 (1997).
[24] B. V. Derjaguin, Colloids Surf., A **79**, 1 (1993).
[25] N. V. Churaev, S. A. Bardasov, and V. D. Sobolev, Colloids Surf., A **79**, 11 (1993); N. V. Churaev, *ibid.* **79**, 25 (1993).
[26] P. Kékicheff and O. Spalla, Langmuir **10**, 1584 (1994).
[27] S. Nir and C. S. Vassilieff, in *Thin Liquid Films: Fundamental and Applications*, edited by I. B. Ivanov (M. Dekker Inc., New York, 1988), pp. 207–274.
[28] J. N. Israelachvili, *Intermolecular and Surface Forces* (Academic Press, London, 1989), pp. 249–250.
[29] H.-J. Butt, Biophys. J. **60**, 777 (1991).
[30] O. Teschke, R. A. Douglas, and T. A. Prolla, Appl. Phys. Lett. **70**, 1977 (1997).
[31] T. J. Senden and C. J. Drummond, Colloids Surf., A **94**, 29 (1995).
[32] R. J. Hunter, *Foundations of Colloid Science* (Clarendon, Oxford, 1989).
[33] J. E. Sader, I. Larson, P. Mulvaney, and L. R. White, Rev. Sci. Instrum. **66**, 3789 (1995).
[34] L. Bergström and E. Bostedt, Colloids Surface **49**, 183 (1990); D. L. Harame, L. J. Bousse, J. D. Shott, and J. D. Meindl, IEEE Trans. Electron Devices **34**, 1700 (1987).
[35] C. J. Drummond and T. J. Senden, Colloids Surf., A **87**, 217 (1994).
[36] R. M. Sassaki, R. A. Douglas, M. U. Kleinke, and O. Teschke, J. Vac. Sci. Technol. B **14**, 2432 (1996).
[37] W. A. Ducker, T. J. Senden, and R. A. Pashley, Langmuir **8**, 1831 (1992); H.-J. Butt, M. Jaschke, and W. A. Ducker, Bioelectrochem. Bioenerg. **38**, 191 (1995).
[38] O. Teschke and E. F. Souza, Appl. Phys. Lett. **74**, 1755 (1999).
[39] R. Becker and F. Sauter, *Electromagnetic Fields and Interactions* (Dover, New York, 1982); O. Teschke, E. F. Souza, and G. Ceotto, Langmuir **15**, 4935 (1999).
[40] Y. Gur, I. Ravina, and A. J. Babchin, J. Colloid Interface Sci. **64**, 333 (1978).

[41] R. Podgornik, G. Cevc, and B. Zeks, J. Chem. Phys. **87**, 5957 (1987).
[42] P. Kékicheff, H. K. Christenson, and B. W. Ninham, Colloids Surface **40**, 31 (1989).
[43] O. Teschke, G. Ceotto, and E. F. de Souza, Chem. Phys. Lett. **326**, 328 (2000).
[44] M. Odelius, M. Bernasconi, and M. Parrinello, Phys. Rev. Lett. **78**, 2855 (1997).
[45] W. R. Fawcett, J. Chem. Phys. **93**, 6813 (1990).